The Understanding of the Microstructural Changes of Refractory Castables after Thermal Shocks through Damping Measurements

N. Traon, Th. Tonnesen, R. Telle

The work herein correlates the damping measurements and the microstructural modifications of refractory castables after thermal shocks at air. According to DIN EN 993-11, thermal shock at air at different temperatures (750, 850, 950 and 1050 °C) were progressively conducted on refractory samples based on tabular alumina with addition of partially stabilized zirconia (PSZ). The same thermal shocks were carried out at 950 °C on white fused alumina samples as well. The thermal shock damage evaluation of high-alumina refractory castables was based on dynamic Young's modulus and damping characterization data obtained via the impulse excitation technique (IET), according to the ASTM E1876-07. Scanning Electron Microscopy (SEM) completes this survey so as to understand the elastic changes of these refractory formulations. The results show that the damping increase in PSZ castables may be explained by crack nucleation and propagation while such phenomena do not occur in WFA castable.

1 Introduction

The service life evaluation and improvement of refractory castables for applications in the metallurgical or the iron and steel industry with regard to physical aspects like thermal shocks and chemical ones like corrosive reactions is continuously investigated. The choice of available raw materials for high performance castables with excellent strength and thermo-mechanical properties plays a central role in the refractory field and are still directed towards this service life optimization. The thermal shock resistance is currently determined by the assessment of the retained Young's modulus after each thermal shock cycle with the help of the non destructive impulse excitation technique (IET). However this standardised method provides only few information about the elastic changes of refractory castables samples which were submitted to progressive thermal shocks. A severe depletion of the modulus of elasticity (MOE) is noticeable during crack nucleation followed by a smooth decrease of this elastic property corresponding to the crack propagation [1]. Damping measurements turn out to be more sensitive than those of modulus of elasticity. Such measurements display a great usefulness in homogeneous materials as for the determination of phase transformation or microstructural modification like macro or microscopic crack formation, thermally activated reorientation of elastic dipoles by the movement of oxygen vacancies, etc [2]. The characterization of such phenomena is more accurate for homogeneous structural ceramics. Nevertheless the interpretation of damping changes of brittle materials with heterogeneous microstructure such as refractory materials is more challenging. Their micro-structure can be seen as anisotropic hard grains and aggregates or crystals consolidated by a mesoscopic bond system containing every kind of defects like cracks, frictional contacts and dislocations at the grain boundaries [3]. This complex material configuration is responsible for non linear effects that make the damping measurements more scattering since the defect density within the material is high. Because of the thermal expansion mismatch between the grog grains and the matrix, cracks are nucleating at the level of the grain boundaries and propagating throughout the matrix increasing subsequently the defect density in the castable's microstructure and moreover the non linear response with the number of thermal shock cycles. This non linear elasticity has already been the subject of surveys conducted on rocks presenting a microstructure similar to that of concrete [4, 5]. Even so, the study of damping measurement changes combined together with SEM analyses lead to the understanding and the quantifying of the role of the defined microstructural changes in the depletion of elastic properties.

Furthermore, to attain a suitable performance during refractory application, aggre-

Nicolas Traon, Thorsten Tonnesen, Rainer Telle
GHI/RWTH-Aachen
Institute of Mineral Engineering – Department of Ceramics and Refractory Materials
52062 Aachen
Germany

Corresponding-Author: *Nicolas Traon*
E-mail: traon@ghi.rwth-aachen.de

Keywords: thermal shock, impulse excitation technique, partially stabilized zirconia, Young's modulus, damping

Received: 06.10.2011
Accepted: 24.10.2011

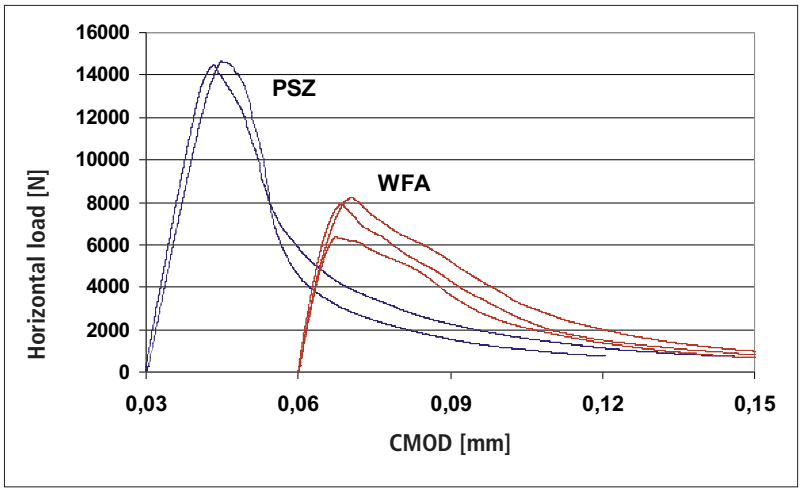

Fig. 1 Horizontal load x CMOD displacement-curves of both studied castable formulations (Source: B. Schickle et al., 53rd International Colloquium on Refractories, Aachen, Germany [2010])

gates of white fused alumina, tabular alumina, sintered pre-formed spinel, magnesia or partially stabilized zirconia are commonly added to calcium aluminate cement (CAC) bonded refractory formulations [6, 7]. The main focus of this study will be stressed on monocrystal of white fused alumina presenting theoretically a high isotropy compared to that of tabular alumina for instance, and on partially stabilized zirconia added as aggregate in a tabular alumina based formulation. The martensitic transformation of this last mentioned raw material coming with a non negligible volume expansion (3–5 %) occurs at 1170 °C. Indeed tetragonal grains of partially stabilized zirconia apply radial stresses in the matrix, so that cracks have to bypass these grains by propagating. In addition to this, the energy of crack propagation can be absorbed by these tetragonal grains transforming into monoclinic ones. The induced volume expansion can lead to cracks' clos-ure in that case. To limit the effects of grain size distribution on elastic properties measurements, aggregates with a maximum size of 3 mm will be used in both formulations.

As documented in Fig. 1, both studied castable formulations do not present the same behaviour with regard to the energy of fracture examined by wedge splitting test [8]. Thus the formulation based on partially stabilized zirconia (PSZ) withstands high horizontal load with a low displacement and the resistance to the sample fracture drastically decreases. Such an evolution is typical of materials that present a high resistance to crack initiation and a low resistance to crack propagation. Thus such castables can withstand high load while cracks are propagating throughout the microstructure till the crack density has reached a threshold and the grains of partially stabilized zirconia are not able anymore to absorb the energy of the propagation of cracks. On the other hand, the formulation constituted of electrofused alumina (WFA) does not withstand such a high horizontal load but the resistance to the sample fracture slowly decreases with a broaden displacement. That evolution is characteristic of materials that present a low resistance to crack formation and a high resistance to crack propagation. In that case the porosity of the castable is able to absorb the energy of the propagation of cracks till the complete splitting of the sample.

From this wedge splitting test, the fracture energy of both materials has been estimated at 105,3 J/m² concerning PSZ and at 68,6 J/m² as far as WFA is concerned. The fracture energy is an important parameter for the characterization of resistance to thermal shocks. According to Hasselman, thermal shock parameters are grouped according to whether they applied to crack initiation or propagation. Equations 1 and 2 represent respectively thermal shock parameters applied to crack initiation and crack propagation:

$$R = \frac{\sigma_c (1-\upsilon)}{\alpha E} \quad [°C] \qquad (1)$$

$$R''' = \frac{E.G_f}{\sigma_c^2 (1-\upsilon)} \quad [Pa^{-1}] \qquad (2)$$

Thermo-mechanical specific values as well as damage tolerance parameters of the studied materials are summed up in Tab. 1. It is worth mentioning that the same approximate value of coefficient of dilatation has been used for both materials.

The determination of those thermal shock parameters is in agreement with the theory presented from the evolution of the wedge splitting test. WFA castable with a low value of R and a high value of R'''' is more brittle than PSZ castable with a high value of R and a low value of R'''' at room temperature. The focus of this study will also consist in determining if such a behavior with regard to crack initiation and crack propagation can be noticed with help of damping measurement.

Tab. 1 Thermal shock parameters applied to crack initiation and crack propagation of WFA and PSZ refractory castables at room temperature

	Gf [J/m²]	υ	α [K⁻¹]	E [GPa]	σ_c [MPa]	R [°C]	R'''' [m]
WFA	68,6	0,135	≈ 8·10⁻⁶	94,75	18,25	20,8	22,6
PSZ	105,3	0,160	≈ 8·10⁻⁶	104,61	34,38	34,5	11,1

2 Experimental procedure

2.1 Material and thermal shocks

Two high alumina castables were studied. The first one is constituted of tabular alumina (*Rio Tinto Alcan*) and partially stabilized zirconia [PSZ] (*Industriekeramik Hochrhein GmbH/DE*). The second formulation is based on white fused alumina [WFA] (*Rio Tinto Alcan/FR*). The calcium aluminate cement Secar 71 (*Kerneos/FR*) as well as the additives namely the deflocculant (FS 40, *BASF/DE*) and citric acid used as retarder complete both formulations. In both compositions, the maximum grain size of the aggregates was 3 mm. Both formulations obey the same Andreasen packing model with a distribution coefficient of 0,26 for a possible comparison of the thermal shock resistance. Prismatic bars were prepared with dimensions 160 mm × 40 mm × 40 mm.

After being moulded, cured for 48 h in a humid environment and dried at 110 °C for 24 h, the specimens were fired. WFA samples were soaked at 1500 °C for 6 h at a heating and cooling rate of 2 K/min. PSZ samples were soaked at 1300 °C for 6 h at a heating and cooling rate of 1 K/min. A lower firing temperature had to be chosen due to the damage of coarse grains fired at 1500 °C.

Thermal shocks at air were conducted on each sample according to DIN EN 993-11 [9]. Each specimen was submitted to a specific number of progressive thermal shocks from one to ten. The tests were carried out at four different temperatures on PSZ samples: 750 – 850 – 950 and 1050 °C. WFA specimens were only submitted to thermal shocks at 950 °C.

2.2 The impulse excitation technique (IET)

The modulus of elasticity and the damping were measured on each sample after each thermal shock cycle according to ASTM E1876-07 with the help of a Resonant Frequency Damping Analyser (RFDA) provided by *IMCE/BE* [10]. Flexural and torsional mode was used with the purpose of the determination of the Young's modulus, the shear modulus and subsequently the Poisson's ratio as well as the flexural and torsional dampings. In this technique, a specimen subjected to proper mechanical boundary conditions in accordance with the expected mode of vibration is excited by a short and light mechanical impulse. The acoustic response is sensed by a microphone and processed according to the frequency and attenuation rate detection. For bars with square cross-sections excited at the flexural mode of vibration, the Young's modulus (E) is calculated using the following equation:

$$E = 0{,}94642 * \left(\frac{m}{b * R^2}\right) * \left(\frac{l}{h}\right)^3 * T \qquad (3)$$

The parameter R is the Grindo sonic output [µs] and is inversely proportional to the flexural frequency, h is the specimen thickness perpendicular to the vibration direction, l is the specimen length, b is the specimen width and T is a geometrical correction factor that depends on the aspect ratio of the specimen (depending on l and h) and the Poisson's ratio. The shear modulus (G) is calculated in a similar manner from the torsional frequency. The Poisson's ratio (ν) is calculated by the relation $\nu = [(E/2G)–1]$ with an interactive algorithm, which also improves the E and G precision. The damping (ξ) is commonly calculated using the logarithmic decrement method:

$$\xi = \frac{\delta}{\omega} \qquad (4)$$

The parameter δ is the angular coefficient of the specimen's acoustic response attenuation on a logarithmic scale, and ω is the angular frequency.

$$\delta = \frac{1}{r} \ln\left(\frac{A_i}{A_{i+r}}\right) \qquad (5)$$

The parameter A_i corresponds to the amplitude of the peak point in the time sinusoidal signal decay function, A_{i+r} is the amplitude of the peak point r cycles later in the time history.

And for a possible comparison of the results, the same experimental geometric conditions were considered. First of all, an automatic positioning sample holder was used to impose the mechanical boundary condition so that the flexural nodes could be predominantly excited. The distance between the microphone and the samples was kept to 5 mm and the distance between the impulse actuator and the sample was kept to 2 mm. The intensity of the impulse excitation was the same for all samples and previously chosen to minimize eventual non-linearity acoustic response [11]. The sample holder apparatus used in a flexural mode can be seen in Fig. 2.

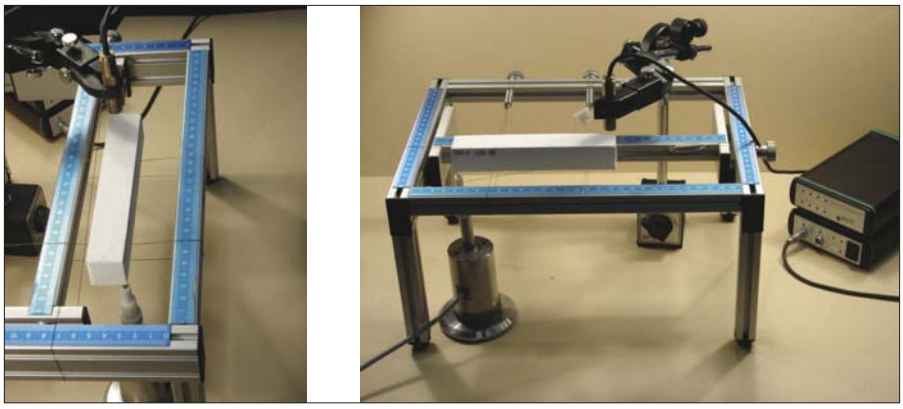

Fig. 2 Flexural mode experimental set up for the determination of elastic properties

3 Results and discussions

3.1 Results and discussions of experiments carried out on PSZ samples

3.1.1. Elastic properties

Fig. 3 shows the retained Young's modulus values of PSZ samples as a function of the number of thermal shock cycles at different tested temperatures (750 – 850 – 950 and 1050 °C). For any thermal shock temperature variation, a two-step decrease of the modulus of elasticity is observed. The two first cycles turn out to be severe enough, so that crack nucleation occurs within the matrix and causes the depletion of the elastic property. This decrease is all the more noticeable that the magnitude of temperature change is high. Thus after the whole series of tests, the higher the thermal shock temperature variation, the lower the retained elastic property. Thermal shock at air at 1050 °C is so severe that the measurement of the elastic properties reveal high scatters after the last and tenth cycle. After ten thermal shock cycles, the retained modulus of elasticity is the highest for a thermal shock temperature change (ΔT) of 750 °C with 82,5 % followed by a ΔT of 850 °C, 950 °C and 1050 °C after nine thermal shock cycles for the last mentioned case with respectively 74 %, 57 % and finally 43,5 %. It is worth to mention that the Young's modulus evolution of 750 °C and 850 °C follow the same tendency while that of 950 °C and 1050 °C stand out from the two first quoted curves. This thermal shock temperature variation of 950 °C is therefore higher than the critical temperature difference defined by *Hasselman* and leads to crack nucleation, crack propagation and cracks' unification [12].

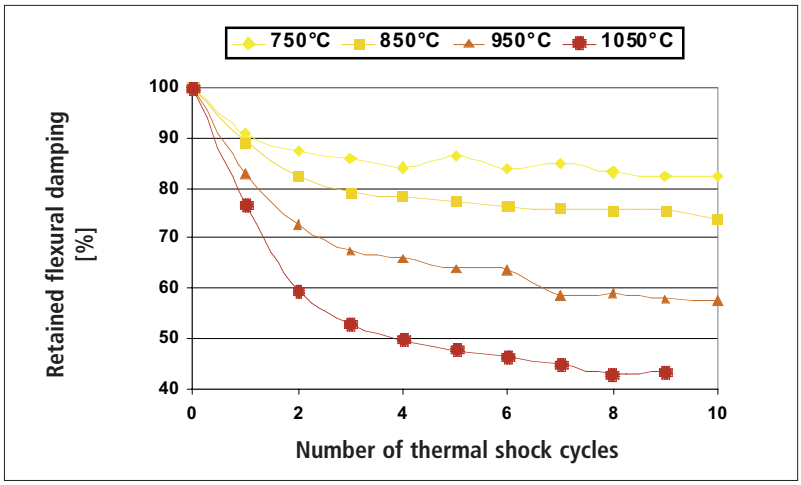

Fig. 3 Evolution of the retained Young's modulus of PSZ castable with the number of thermal shock cycles at different tested temperatures (750 – 850 – 950 and 1050 °C)

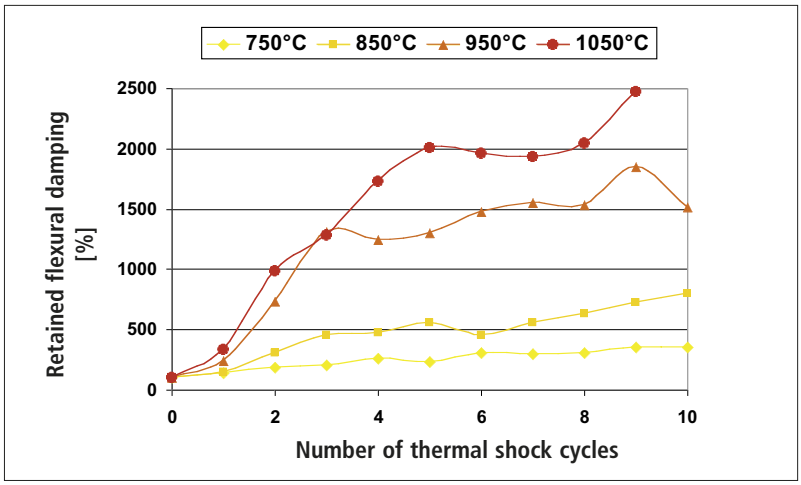

Fig. 4 Evolution of the retained flexural damping of PSZ castable with the number of thermal shock cycles at different tested temperatures (750 – 850 – 950 and 1 050 °C)

Fig. 4 shows the retained flexural damping values of PSZ samples as a function of the number of thermal shock cycles at different testing temperatures (750 – 850 – 950 and 1050 °C). As expected, the damping changes follow the inverse tendency of the retained Young's modulus and increase with the formation of cracks and microcracks. The more the cracks are propagating within the matrix, the higher the damping. Thus after the whole series of tests, the higher the magnitude of temperature change the higher the retained flexural damping. After ten thermal shock cycles, the retained flexural damping is lower for a thermal shock temperature variation (ΔT) of 750 °C with 360 % followed by a ΔT of 850 °C, 950 °C and 1050 °C after nine thermal shock cycles for the last mentioned case with respectively 800 %, 1500 % and finally 2500 %. Damping values do not change as a two-step process. Indeed damping increases with the damage increase at low thermal shock temperature variations (750 and 850 °C) but turns out to be more difficult to be modelled at higher thermal shock temperature differences (950 and 1050 °C). Experiments carried out at a thermal shock temperature change of 1050 °C combined with the microstructure examin-ation leads to the conclusion of a four-step evolution of the microstructural changes. Up to and including the second cycle, crack nucleation at the level of the grain boundaries causes the first increase of the damping measurements up to 1000 %. The second increase reaching 2000 % of the initial value occurring up to and including the fifth cycle can be explained by the propagation of the cracks within the matrix and throughout the Al_2O_3 aggregates. This step is followed by a steady state up to and including the eighth cycle while cracks have to consume a lot of energy in order to bypass the ZrO_2 aggregates. Finally cracks' unification occurs during the ninth cycle, this cracks' network explains the depletion of the elastic properties and the further difficulties to achieve realistic damping values over 2500 % of the initial value.

3.1.2 Microstructure examination

The microstructure of the studied castables has been examined by means of SEM analyses on polished samples after each thermal shock. Figs. 5-8 represent the homogeneous distribution of zirconia grains and Al_2O_3 aggregates in the matrix made of hibonite crystals or calcium hexaaluminate CA_6 particles and monocalcium dialuminate CA_2. The small amount of facets CA_6 in the microstructure because of a low sintering temperature indicates that the PSZ matrix is in majority constituted of CA_2 particles. Because of the thermal expansion mismatch between the grog grains and the matrix, cracks are nucleating at the level of the grain boundaries after the sintering and the first thermal shock cycle, as it can be seen in Fig. 5.

The second step of microstructural changes is illustrated in Fig. 6. After propagating along the grain boundaries and within the matrix, which is much more fragile than the aggregates, the cracks are henceforth able to propagate throughout the grog grains of alumina. Tabular alumina grains contain a non negligible inner porosity and inclusions of Na_2O. From this physical statement, the crack propagation within Al_2O_3 grog grains is made easier.

Then cracks have to bypass the zirconia grains that apply radial stresses in the matrix, as shown in Fig. 7. This crack bridging phenomenon consumes a lot of energy and is responsible for the martensitic transformation of tetragonal grains into monoclinic ones sometimes causing crack closure. Microcracks are formed from this transformation characterized by a volume expansion at the level of the grain boundaries. Those microcracks can later absorb the energy of another crack's propagation. The combination of these mechanisms can explain the steady state of damping changes witnessing the ability of such a refractory formulation to counter the damaging of the sample.

After nine thermal shocks the crack density within the sample's microstructure is so high that cracks can get unified. In addition to this, those cracks are henceforth able to progress throughout the zirconia grains, as illustrated in Fig. 8. That explains the sudden depletion of the elastic properties and the irreversible damaging of the samples. Thus, damping measurements are difficult to be monitored.

3.2 Results and discussions of experiments carried out on WFA samples

3.2.1 Elastic properties

Fig. 9 shows the evolution of the retained modulus of elasticity and the retained flexural damping of WFA samples as a function of the number of thermal shock cycles at air at 950 °C. The Young's modulus follows the same tendency as that of PSZ, in other words a strong decrease of this property is noticeable up to 70 % after just one thermal shock followed by a smooth decrease till the end of the experiment up to 40 %. However this property depletion is more important for WFA than for PSZ at the same tested temperature: that shows the relevance of the addition of partially stabilized zirconia grains in a standard formulation, and more stable and more thermal shock resistant interfaces between matrices and aggregates in the tabular alumina based formulation compared to that based on white fused alumina with regard to this kind of thermal shock at air. It is worth to mention that a more important decrease appear after the eighth thermal shock cycle which is in correlation with an important increase of the damping values. Damping evolution can nevertheless follow several models of interpretation: damping may proportionally increase with the number of thermal shock cycles. Taking into account the uncertainty of the measurement, damping values oscillate around a proportional model in that case. A logarithmic evolution is nevertheless conceivable: damping values strongly increase during the first submitted thermal shock cycles and then this increase is not so notable.

3.2.2 Microstructure examination

The aggregates of white fused alumina as an electro-fused raw material present a low inner porosity, as shown in Fig. 10. This raw material with a very low specific surface area is not as reactive as tabular alumina which corresponds to a sintered raw material. That is the reason why the connection between the dense grains of alumina is really low: the edges of the grains are straight and open gaps between matrix and aggregates are obvious.

After ten thermal shock cycles, the grog grains of white fused alumina present a non negligible inner porosity. Contrary to the PSZ formulation, the stresses induced by the temperature difference of the thermal shock do not cause any crack nucleation within the matrix because of this obvious low degree of connection between the grains. The damaging of the largest crystals of alumina may be mainly responsible for the damping's increase as shown in Fig. 11.

Moreover it should be noticed that WFA castable apparent porosity is much higher than that of PSZ (18,9 % for PSZ against 20,0 % for WFA). This difference is essentially due to the low reactivity of electrofused

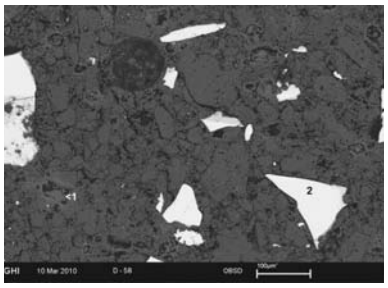

Fig. 5 Crack nucleation at grain boundaries of PSZ castable after one thermal shock cycle at air at 1050 °C

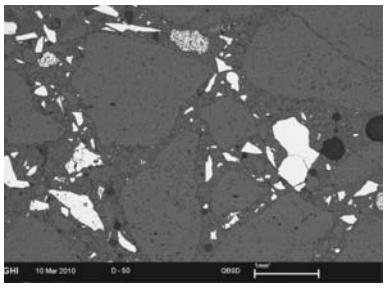

Fig. 6 Crack propagation within the matrix and throughout the Al_2O_3 aggregates of PSZ castable after three thermal shock cycles at air at 1050 °C

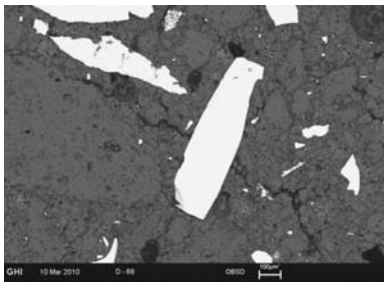

Fig. 7 Crack deviation along zirconia grains of PSZ castable after five thermal shock cycles at air at 1050 °C

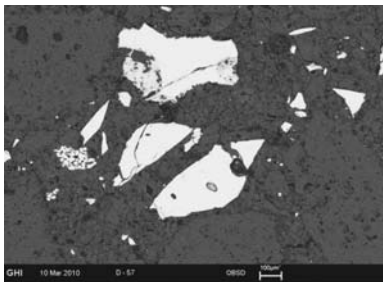

Fig. 8 Cracks' unification and crack propagation throughout ZrO_2 aggregates of PSZ castable after nine thermal shock cycles at air at 1050 °C

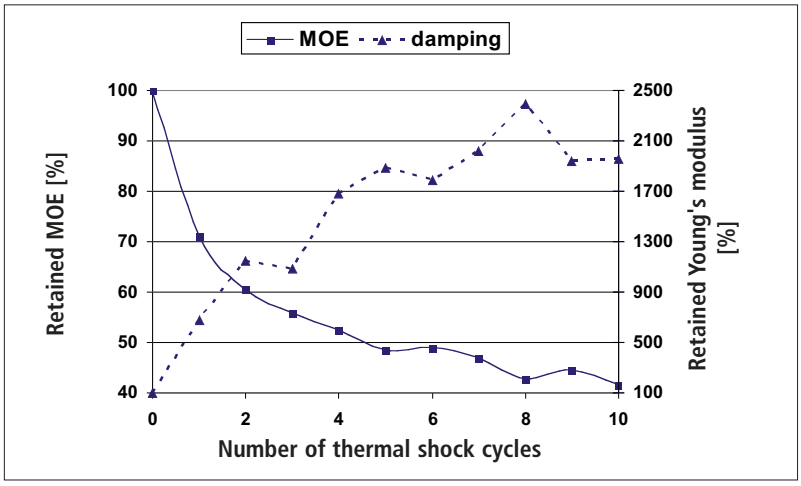

Fig. 9 Evolution of the retained Young's modulus and the retained flexural damping of WFA castable with the number of thermal shock cycles at 950 °C

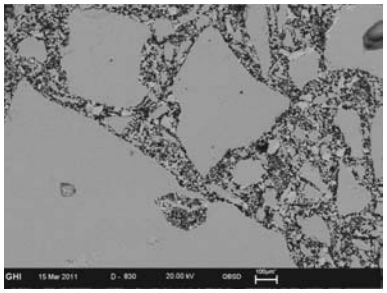

Fig. 10 Microstructural overview of WFA sample after one thermal shock cycle at air at 950 °C

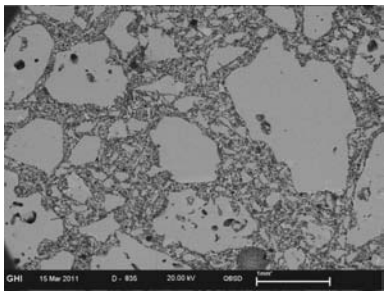

Fig. 11 WFA aggregate damaging after ten thermal shock cycles at air at 950 °C

grains that results in the low degree of connection between the grains, while the packing model before sintering is the same as PSZ. In such a microstructural configuration, the aggregates of white fused alumina allow themselves a higher liberty of movement that entails a higher damping value after sintering ($429 \cdot 10^{-6}$ for WFA against $389 \cdot 10^{-6}$ for PSZ). From this standpoint, the internal friction is subsequently higher after a mechanical solicitation.

4 Conclusions

The evolutions of the retained Young's modulus and the flexural damping with the number of thermal shock cycles are strongly correlated. The lower the Young's modulus, the higher the damping. However the damping evolution turns out to bring more information about the microstructural changes. This statement is documented by SEM analyses.

Thus in formulation presenting a high degree of connection between the grains and an optimal packing model like PSZ formulation, damping values evolution may be explained by a defined sequence of microstructural changes:

- crack formation at the level of the grain boundaries
- crack propagation within the matrix and throughout the Al_2O_3 aggregates
- crack deviation by partially stabilized zirconia grains
- cracks' unification and crack propagation throughout ZrO_2 grains.

In formulation with a higher open porosity like WFA formulation, the interpretation of the damping changes is more challenging. In that case, cracks can not nucleate and propagate within the matrix because of a low degree of connection between the grains. Therefore the induced stresses lead to the damaging of the grog grains and the energy provided by those thermo-mechanical stresses is partially absorbed by the open porosity. Besides this high porosity and homogeneous distribution of the pores lead to an increase of the internal friction and higher nominal damping values and to dissipation of the energy.

Thermal shock parameters determination leads to the classification of the materials according to whether they are resistant to crack initiation or crack propagation. Damping measurements lead to the identification of the microstructural changes in dense refractory materials and reveal the degree of liberty of movement of aggregates in porous materials. Therefore the examination of the microstructure turns out to be necessary as for the interpretation of this elastic characteristic. Nevertheless damping shows the microstructural damage that could not be detected neither by SEM nor with help of Young's modulus assessment. Damping measurements bring information at high level of damage while the modulus of elasticity and the resistance to horizontal load do not show any change.

Non linear effects caused by crack formation and anisotropy of the aggregates are all the more important that the defect density is high. Therefore damping measurements have to be carefully interpreted according to the quantity of thermal stresses induced by the thermal shock procedure.

Acknowledgements

The authors would like to express their sincere thanks to the *DFG Project* "Evaluation of the damage on refractory materials after thermal shocks through the measurement of the damping and of the resonant frequency" *within the framework of SPP 1418 (reference number: TE 146/30-1)* for the financial support.

References

[1] Tonnesen, T.; Telle, R.: Thermal shock damage in castables: Microstructural changes and evaluation by a damping method. cfi/Ber. DKG 84 (2007) [9] E132–136.

[2] Mielczarek, A.; Fischer, H.; Riehemann, W.: Amplitude-dependant damping of PSZ with sinter defects. Mater. Sci. Engin. A 442 (2006) 488–491

[3] Pereira, H.A.; Nascimento, R.C.; Rodrigues, J. de A.: Effect of non linearity on Young's modulus and damping characterisation of high alumina refractory castables through the impulse excitation technique. 53rd Int. Coll. on Refractories (2010) Aachen, Germany, Proc. 90–93

[4] Johnson, P.A.; Zinszner, B.; Rasolofosaon, N.J.: Resonance and elastic nonlinear phenomena in rock. J. Geophys. Res. 101 (1996) [B5] 11553–11564

[5] Abeele, K.V.D.; Visscherb, J.: Damage assessment in reinforced concrete using spectral and temporal nonlinear vibration techniques. Cement and Concrete Res. 30 (2000) 1453–1464.

[6] Braulio, M.A.L.; et al.: Aggregate effects on the thermal shock resistance of spinel-forming refractory castables. Refractories Worldforum (2010) [2] 102–106

[7] Primachenko, V.; et al.: The influence of sintered or fused MgO-stabilized ZrO_2 on properties of zirconia products. Proc. UNITECR 2007 (2007) 268–271

[8] Schickle, B.; Telle, R.; Tonnesen, T.: Changes of the mechanical and elastic properties of castables as a function of thermal shock cycles. 53rd Int. Coll. on Refractories (2010) Aachen, Germany, Proc. 86–89

[9] DIN EN 993-11: Determination of resistance to thermal shock, German version CEN/TS 993/11 (2003)

[10] ASTM 1876-07: Standard test method for dynamic Young's modulus, shear modulus, and Poisson's ratio by impulse excitation of vibration. ASTM International (2007) 15

[11] Pereira, H.A.; et al.: Elastic moduli, damping and modulus of rupture changes in a refractory castable due to thermal shock damage. 52nd Int. Coll. on Refractories (2009) Aachen, Germany, Proc. 20–23

[12] Hasselman, D.P.H: Rolle der Bruchzähigkeit bei der Temperaturwechselbeständigkeit feuerfester Erzeugnisse. Ber. DKG 54 (1954) 195–201